Laser cooling at low intensity in a strong magnetic field

P. van der Straten
Vakgroep AGF, Fysisch Laboratorium, Rijksuniversiteit Utrecht, Postbus 80000, 3508 TA Utrecht, The Netherlands

S-Q. Shang,*, B. Sheehy,† and H. Metcalf
Department of Physics, State University of New York, Stony Brook, New York 11794

G. Nienhuis
Huygens Laboratorium, Rijksuniversiteit Leiden, Postbus 9504, 2300 RA Leiden, The Netherlands
(Received 17 April 1992)

We have studied theoretically and experimentally the effect of a relatively strong magnetic field on sub-Doppler laser cooling in a one-dimensional optical molasses. We used the operator description of laser cooling with the Larmor precession frequency ω_Z being much higher than the optical pumping rate. We found velocity-selective resonances (VSR) in the force at velocities $v_r = n\omega_Z/K$, with $n = 0, \pm 1, \pm 2$ for both the scattering and redistribution force operators. These depend on the relative direction of the magnetic field and the polarization vectors of the light beams. Analytical results for the force on the atom are obtained in two cases that illustrate the effect of the VSR on the force. These formulas are compared with numerical calculations of the force. We also discovered a redistribution mechanism that relies on the gradient of the eigenstates of the light-shift operator, with eigenvalues that are independent of position so that a "Sisyphus cooling" picture does not apply. The theory is compared with many experimental results and excellent agreement is found. We believe that all essential features of laser cooling at low intensity are well described by this operator theory.

PACS number(s): 32.80.Pj, 42.50.Vk

I. INTRODUCTION

Laser cooling of neutral atoms has been the subject of many different studies. The experimental discovery of sub-Doppler laser cooling (SDLC) [1] has spurred very much attention to this field, and SDLC has now been studied in many experiments. Early theoretical descriptions [2, 3] attributed the SDLC to polarization gradients that are always present in three-dimensional optical molasses. Although these theories are one dimensional, it is commonly accepted that the polarization gradients in combination with the multiplicity of the ground state are indeed responsible for SDLC in three dimensions. In the one-dimensional lin $\perp$ lin scheme [2], where the counterpropagating beams are linearly polarized in the orthogonal directions, atoms are optically pumped between different light-shifted ground states, and the polarization gradient causes the population of the sublevels of moving atoms to be mixed. This causes a velocity-dependent exchange of kinetic and potential energy that produces a damping force. Experiments were performed that confirmed these models [4].

It was also realized that a magnetic field could cause populations of the sublevels to be mixed and subsequent one-dimensional (1D) optical molasses experiments produced SDLC using both low [5] and high [6] magnetic fields in the absence of a polarization gradient. These experiments led to the velocity-selective resonance (VSR) picture of SDLC processes [7]. VSR can occur between two ground-state magnetic sublevels if the energy difference between them is compensated by the Doppler shifts of the laser frequencies of the two counterpropagating laser beams. These VSR's also have a profound effect on laser cooling experiments that do have polarization gradients [7–9] and the VSR picture studied in one-dimension provided a way of unifying the description of all these processes [7].

We have been studying SDLC processes in a uniform **B** field and have developed theoretical models to describe our experiments [5–7]. Furthermore, we have presented a more formal description of these experiments that is valid for arbitrary transition schemes at low **B** field (e.g., $B \sim 0.1$ G) [10, 11]. At higher **B** fields (e.g., $B \sim 1$ G) we find new phenomena such as cooling of atoms to a nonzero velocity [6, 7, 12]. The magnetic field scale is always set by the requirement that the Zeeman frequency ω_Z be small compared with the excited state decay rate Γ.

We use our previously described apparatus [5–7] to produce a thermal beam of natural Rb crossed by a pair of counterpropagating laser beams transverse to the atomic beam axis. The atomic-beam profile is measured with a scanning hot tungsten wire, 25 μm in diameter, 1.3 m away from the region of interaction with the laser beam. Three square Helmholtz coil pairs provide a controlled magnetic field **B** (see Fig. 1).

For small magnetic fields we observed 1D atomic velocity distributions centered at $v = 0$ with spreads as low as 2 cm/s when we cooled Rb on the $\lambda \equiv 2\pi/K = 780$ nm transition [5] (see Fig. 2). This is much lower than the one-dimensional Doppler limit $v_D = (7\Gamma/20k_B)^{1/2}$ (= 10

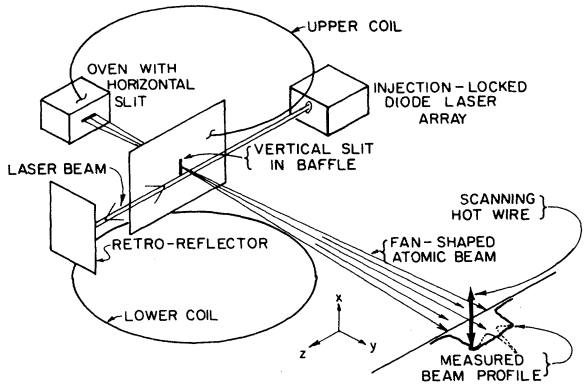

FIG. 1. Schematic diagram of apparatus.

cm/s, for Rb). Here $\Gamma \equiv 1/\tau$ ($= 2\pi \times 6$ MHz for Rb) is the natural width of the excited state. At fields near 1 G, we observed cooling of atoms to nonzero velocity [6, 7]. Velocity selective resonances cause the population difference and coherences between the ground-state atomic sublevels to change rapidly near the resonance velocity $\pm v_r$ and therefore produce a strong damping of the atoms to this resonance velocity.

In this paper we present a description of these higher field processes. We extend the theory of operator description of sub-Doppler laser cooling [11] to the case of strong magnetic field. The optical pumping process can then be treated as a perturbation to the Larmor precession in the magnetic field. This leads to the identification of velocity selective resonances, where the optical pumping process strongly couples two ground magnetic substates. In Sec. II we present the formalism and derive expressions for the force for the different resonances. In Sec. III we compare the results with our measurements.

II. THEORY

A. Force on atoms in the low-intensity limit

In order to fix the notation we briefly recapitulate the results of our previous paper [11]. We consider an atom moving through a monochromatic radiation field of frequency ω. The field drives the transition between a lower state $|\, g\rangle$ with angular momentum J_g, and an excited state $|\, e\rangle$ with angular momentum J_e, whose energy separation is $\hbar\omega_0$. The optical electric field is expressed as

$$\mathbf{E}(\mathbf{R},t) = \mathbf{E}^{+}(\mathbf{R})e^{-i\omega t} + \mathbf{E}^{-}(\mathbf{R})e^{i\omega t}. \tag{1}$$

It is convenient to separate the atomic density matrix into the submatrices σ_{ee} for the excited level, σ_{gg} for the ground level, and σ_{eg} and σ_{ge} for the optical coherences between them. Likewise, the electric dipole operator $\boldsymbol{\mu}$ can be separated in the submatrices $\boldsymbol{\mu}_{eg}$ and $\boldsymbol{\mu}_{ge}$. (The diagonal parts $\boldsymbol{\mu}_{ee}$ and $\boldsymbol{\mu}_{gg}$ vanish when $|\, e\rangle$ and $|\, g\rangle$ have a definite parity.) In the rotating-wave and the dipole approximations, the atom-field coupling is described by the Rabi operator

$$\mathcal{R} = \boldsymbol{\mu}_{eg} \cdot \mathbf{E}^{+}(\mathbf{R})/\hbar, \tag{2}$$

which has the dimensions of a frequency. For an atom of given velocity $\mathbf{v}$, the coupling (2) depends on time through the time-dependent atomic position $\mathbf{R}(t) = \mathbf{R}_0 + \mathbf{v}t$.

The gain in the ground-state population from spontaneous decay of the excited state is conveniently described in terms of the reduced dimensionless dipole operator $\boldsymbol{\mathcal{Q}}$, which has the spherical components

$$\mathcal{Q}_\beta = \mathbf{u}_\beta \cdot \boldsymbol{\mathcal{Q}} \tag{3}$$

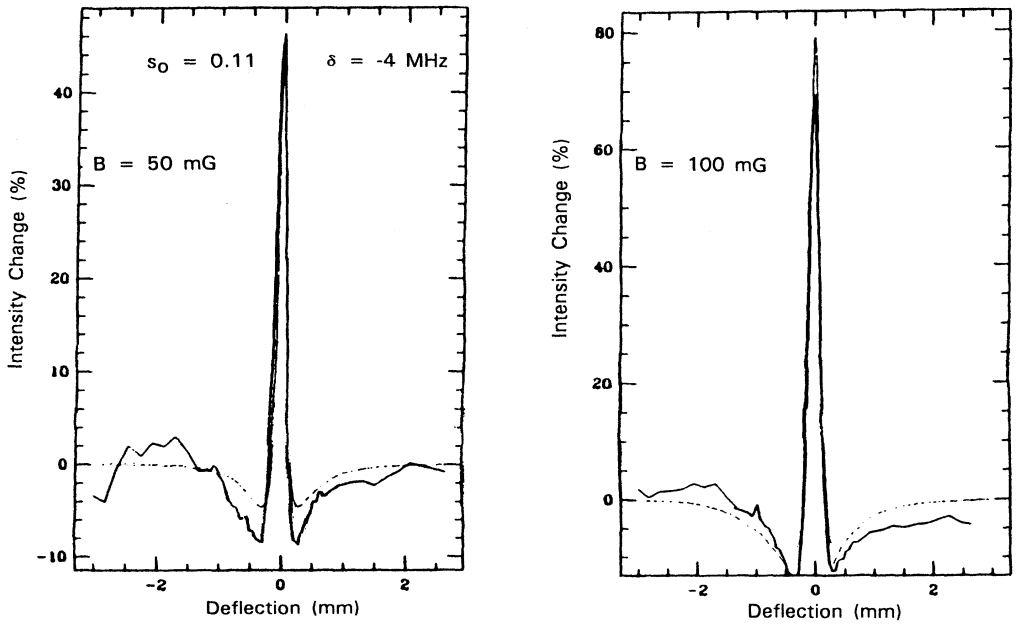

FIG. 2. The atomic beam profile measured with the scanning hot wire in the MILC configuration. The laser intensity $I = 0.3I_{\rm sat}$, the detuning $\Delta = -4$ MHz, and the field was 50 mG (left) and 100 mG (right).

with

$$\mathbf{u}_{-1} = (\hat{\mathbf{X}} - i\hat{\mathbf{Y}})/\sqrt{2}, \quad \mathbf{u}_0 = \hat{\mathbf{Z}}, \quad \mathbf{u}_1 = -(\hat{\mathbf{X}} + i\hat{\mathbf{Y}})/\sqrt{2} \tag{4}$$

the spherical unit vectors. The normalization of $\mathcal{Q}$ is fixed by requiring that the matrix elements of its spherical components are Clebsch-Gordan coefficients as described by [13]

$$\langle J_e M_e \mid \mathcal{Q}_\beta \mid J_g M_g \rangle = \langle J_e M_e \mid J_g M_g; 1\beta \rangle, \tag{5}$$

for $\beta = -1, 0, 1$. The values $\beta = \pm 1$ correspond to two opposite circular polarizations in the XY plane, and the value $\beta = 0$ corresponds to linear polarization along the Z axis.

We consider the low-intensity limit, where the rate of stimulated transitions is much lower than the natural linewidth Γ. Furthermore, we assume that the atomic velocity is so low that the Doppler shift ω_D is small compared with the natural width, so that

$$\omega_D \equiv \mathbf{K} \cdot \mathbf{v} << \Gamma. \tag{6}$$

The combined assumption of low intensity and low velocity is an important ingredient of configurations for sub-Doppler cooling [2]. Finally, we allow for the presence of a uniform external magnetic $\mathbf{B} = B\hat{\mathbf{n}}$, with $\hat{\mathbf{n}}$ a unit vector. The ground-state Larmor precession frequency ω_Z corresponding to this magnetic field is assumed small compared with the natural width, and we have

$$\omega_Z << \Gamma. \tag{7}$$

As we demonstrated in a previous paper [11], in this combined limit of low velocity, low intensity, and low magnetic field the evolution equation for the ground-state density matrix σ_{gg} can be given in closed form after adiabatically eliminating the excited state. The result can be expressed in the form

$$\frac{d}{dt}\sigma_{gg} = \mathcal{G}\sigma_{gg} - (\mathcal{P} + i\mathcal{S})\sigma_{gg} - \sigma_{gg}(\mathcal{P} - i\mathcal{S}) - i\omega_Z[\mathbf{J}_g \cdot \hat{\mathbf{n}}, \sigma_{gg}] \tag{8}$$

with

$$\mathcal{G}\sigma_{gg} = \frac{\Gamma}{\Gamma^2/4 + \Delta^2} \sum_\beta \mathcal{Q}_\beta^\dagger \mathcal{R} \sigma_{gg} \mathcal{R}^\dagger \mathcal{Q}_\beta \tag{9}$$

and $\Delta \equiv \omega - \omega_0$ the detuning of the laser from atomic resonance. The Hermitian operators $\mathcal{P}$ and $\mathcal{S}$ are defined by

$$\mathcal{P} + i\mathcal{S} = \frac{1}{\Gamma/2 - i\Delta} \mathcal{R}^\dagger \mathcal{R}. \tag{10}$$

The operator $\hbar\mathcal{S}$ in (8) plays the role of an effective Hamiltonian, describing the perturbation by the radiation field of the energy levels of the ground state. Its eigenvalues are the light shifts.

The effect of optical pumping is described by a master equation, where $\mathcal{G}$ is the gain term resulting from feeding of the ground state by optical pumping, and $\mathcal{P}$ is the loss. These two operators have a dissipative nature. One readily checks that

$$\gamma_P \equiv 2\,\mathrm{Tr}(\sigma_{gg}\mathcal{P}) = \frac{\Gamma}{\Gamma^2/4 + \Delta^2} \mathrm{Tr}(\sigma_{gg}\mathcal{R}^\dagger \mathcal{R}) \tag{11}$$

is equal to the total rate of optical pumping.

The optical coherences follow the ground-state evolution adiabatically, and they are given by the expressions

$$\sigma_{eg}(t) = \frac{i}{\Gamma/2 - i\Delta} \mathcal{R}(t)\sigma_{gg}(t),$$
$$\sigma_{ge}(t) = \frac{-i}{\Gamma/2 + i\Delta} \sigma_{gg}(t)\mathcal{R}^\dagger(t). \tag{12}$$

These coherences determine the net average force $\mathbf{F}$ exerted on the atom, which is expressed by the average

$$\mathbf{F} = \hbar\langle \boldsymbol{\nabla}\mathcal{R} \rangle + \hbar\langle \boldsymbol{\nabla}\mathcal{R}^\dagger \rangle. \tag{13}$$

From (12) and (13) we obtain the result

$$\mathbf{F} = \mathrm{Tr}(\sigma_{gg}\boldsymbol{\mathcal{F}}) \tag{14}$$

with $\boldsymbol{\mathcal{F}}$ the effective operator

$$\boldsymbol{\mathcal{F}} \equiv \frac{-i\hbar}{\Gamma/2 + i\Delta} \mathcal{R}^\dagger \boldsymbol{\nabla}\mathcal{R} + \frac{i\hbar}{\Gamma/2 - i\Delta} (\boldsymbol{\nabla}\mathcal{R}^\dagger)\mathcal{R}. \tag{15}$$

The prescription for calculating the radiative force is now straightforward. We have to use the effective evolution equation (8) to evaluate σ_{gg}, and the result can be substituted into (14).

The force operator $\boldsymbol{\mathcal{F}}$ can be separated as [11]

$$\boldsymbol{\mathcal{F}} \equiv \boldsymbol{\mathcal{F}}_{\mathrm{red}} + \boldsymbol{\mathcal{F}}_{\mathrm{sc}} \tag{16}$$

into a redistributive part

$$\boldsymbol{\mathcal{F}}_{\mathrm{red}} \equiv \frac{-\hbar\Delta}{\Gamma^2/4 + \Delta^2} \left[\mathcal{R}^\dagger \boldsymbol{\nabla}\mathcal{R} + (\boldsymbol{\nabla}\mathcal{R}^\dagger)\mathcal{R} \right] \tag{17}$$

and a scattering part

$$\boldsymbol{\mathcal{F}}_{\mathrm{sc}} \equiv \frac{-i\hbar\Gamma/2}{\Gamma^2/4 + \Delta^2} \left[\mathcal{R}^\dagger \boldsymbol{\nabla}\mathcal{R} - (\boldsymbol{\nabla}\mathcal{R}^\dagger)\mathcal{R} \right]. \tag{18}$$

The force $\boldsymbol{\mathcal{F}}_{\mathrm{sc}}$ has a dissipative nature, and results from the scattering of photons into the vacuum. The redistributive force $\boldsymbol{\mathcal{F}}_{\mathrm{red}}$ has a conservative nature, and derives from the gradient of the light shift according to

$$\boldsymbol{\mathcal{F}}_{\mathrm{red}} = -\hbar\boldsymbol{\nabla}\mathcal{S}. \tag{19}$$

This force $\boldsymbol{\mathcal{F}}_{\mathrm{red}}$ arises from coherent transfer of photons between plane-wave modes.

B. Strong magnetic field and velocity selective resonances

We wish to specialize further by considering a magnetic field that is sufficiently strong that the Larmor precession frequency ω_Z is large compared with the pump rate γ_P, while remaining small compared with the inverse lifetime Γ. Thus ω_Z obeys the double inequality

$$\gamma_P << \omega_Z << \Gamma, \tag{20}$$

and the evolution equation (8) remains valid. The Lar-

mor term is then the dominant term and

$$H_0 = \omega_Z \mathbf{J}_g \cdot \hat{\mathbf{n}} \tag{21}$$

serves as the dominant part of the Hamiltonian. Its eigenstates are separated by the Zeeman level splitting. The light shift and the optical pumping can be treated as time-dependent terms driving transitions between the Zeeman eigenstates. The time dependence arises from the motion of atoms in a standing wave.

We expand the radiation field in plane waves, according to the equation

$$\mathbf{E}^+(\mathbf{R}) = \sum_i \mathbf{E}_i^+ \exp(i\mathbf{K}_i \cdot \mathbf{R}). \tag{22}$$

The corresponding expansion of the Rabi operator $\mathcal{R}$ is expressed as

$$\mathcal{R} = \sum_i \mathcal{R}_i \exp(i\mathbf{K}_i \cdot \mathbf{R}), \tag{23}$$

with

$$\mathcal{R}_i = \boldsymbol{\mu}_{eg} \cdot \mathbf{E}_i^+ / \hbar. \tag{24}$$

After substituting (23) in the evolution equation (8), we note that the coupling terms between the Zeeman substates have a time dependence that is composed of harmonic terms oscillating at frequencies $(\mathbf{K}_i - \mathbf{K}_j) \cdot \mathbf{v}$ that arise because $\mathbf{R} = \mathbf{R}_0 + \mathbf{v}t$. Since the strength of the driving perturbation is small compared with the level shifts, we expect resonant enhancement of the coupling when one of these effective frequencies coincides with the frequency separation between two coupled Zeeman levels.

Near such a resonance, each term $\mathcal{R}_j^\dagger \mathcal{R}_i$ in $\mathcal{P}$ or $\mathcal{S}$ only couples two Zeeman states $\mid M\rangle$ and $\mid M'\rangle$ with $\omega_Z(M') - \omega_Z(M) = (\mathbf{K}_i - \mathbf{K}_j) \cdot \mathbf{v}$. This reduces to $(M' - M)\omega_Z = (\mathbf{K}_i - \mathbf{K}_j) \cdot \mathbf{v}$, if the Zeeman splitting is much smaller than the fine and hyperfine splitting. A similar resonant selection in the feeding term $\mathcal{G}$ in (8) leads to coupling between matrix elements of the density matrix σ_{gg} with a difference $(M - M')$ in the Zeeman state by an amount of the order of $(\mathbf{K}_i - \mathbf{K}_j) \cdot \mathbf{v}/\omega_Z$. In general we may expect velocity selective resonances corresponding to transitions between Zeeman levels. These resonances in the radiative force arise for velocity classes obeying the relation

$$\mid (\mathbf{K}_i - \mathbf{K}_j) \cdot \mathbf{v} - n\omega_Z \mid << \omega_Z, \tag{25}$$

for $n = -2, -1, 0, 1, 2$. This condition (25) indicates the velocities where laser cooling may be enhanced by VSR. Since the number n corresponds to the difference of the value of M for two states coupled by $\mathcal{R}_j^\dagger \mathcal{R}_i$, its allowed values will depend on the value of the angular momentum J_g and on the polarizations of the plane waves. This will determine which velocity classes will be cooled in any actual configuration.

C. Two counterpropagating plane waves

For the rest of the paper we focus on the case of two counterpropagating plane waves of equal intensity and arbitrary polarizations in the presence of a magnetic field. The Larmor frequency obeys the inequalities (20). Since the magnetic field gives the strongest coupling, it determines the quantization axis, and we select the Z direction parallel to the magnetic field. The Rabi operator (2) is then separated as

$$\mathcal{R} = \mathcal{R}_1 e^{i\mathbf{K}\cdot\mathbf{R}} + \mathcal{R}_2 e^{-i\mathbf{K}\cdot\mathbf{R}}, \tag{26}$$

with the plane-wave Rabi operators

$$\mathcal{R}_i = \tfrac{1}{2}\Omega \boldsymbol{\epsilon}_i \cdot \boldsymbol{\mathcal{Q}} \tag{27}$$

for $i = 1$ or 2. Ω is the effective Rabi frequency for a single traveling wave and the two polarization vectors are indicated by $\boldsymbol{\epsilon}_i$. The Zeeman substates $\mid M\rangle$ are now the eigenstates of J_{gZ}. Transitions between two Zeeman substates of the ground state and the excited state with $\Delta M = \alpha$ are driven by the polarization components

$$\epsilon_{i\alpha} = \boldsymbol{\epsilon}_i \cdot \mathbf{u}_\alpha^*, \tag{28}$$

so that

$$\boldsymbol{\epsilon}_i \cdot \boldsymbol{\mathcal{Q}} = \sum_\alpha \epsilon_{i\alpha} \mathcal{Q}_\alpha, \tag{29}$$

where the quantities $\mathbf{u}_\alpha$ are defined in Eq. (4). The velocity component of the atom in the direction of $\mathbf{K}$ is denoted as v. From (25) we see that we may expect velocity-selective resonances for velocities v obeying the condition

$$\mid 2Kv - n\omega_Z \mid << \omega_Z \tag{30}$$

for $n = -2, -1, 0, 1, 2$. We now give a separate discussion of these various velocity-selective resonances. In each case we will see that $\mathbf{B}$ dependence of the force arises only through the atomic variables, not through the radiation operators.

1. $n = 0$: $Kv \cong 0$

For $n = 0$, the resonance condition (30) reads

$$\mid 2Kv \mid << \omega_Z. \tag{31}$$

For these small velocities the time dependence of the operators $\mathcal{G}$, $\mathcal{P}$, and $\mathcal{S}$ on the right-hand side of (8) is weak compared with the Larmor precession frequency ω_Z, and we only have to include the coupling between matrix elements with the same off-diagonality $M - M'$. This is clear if we transform the rapid Larmor precession away by introducing the ground-state density matrix ρ_0 for $n = 0$ in the rotating frame

$$\rho_0(t) = \exp[i\omega_Z J_{gZ} t/\hbar] \sigma_{gg}(t) \exp[-i\omega_Z J_{gZ} t/\hbar]. \tag{32}$$

We substitute (32) into (8), and neglect the terms oscillating rapidly at the precession frequency. This implies that, after substituting Eqs. (26), (27), and (29), we retain only terms diagonal in the index of $\mathcal{Q}_\alpha$ and $\mathcal{Q}_\alpha^\dagger$. The resulting equation is

$$\frac{d}{dt}\rho_0(t) = \mathcal{G}_0(t)\rho_0(t) - [\mathcal{P}_0(t) + i\mathcal{S}_0(t)]\rho_0(t) - \rho_0(t)[\mathcal{P}_0(t) - i\mathcal{S}_0(t)], \tag{33}$$

where the operators $\mathcal{G}_0, \mathcal{P}_0$, and $\mathcal{S}_0$ are defined by

$$\mathcal{G}_0\rho_0 = \frac{s_0\Gamma}{2}\sum_\alpha\sum_\beta \mid \epsilon_{1\alpha}e^{iKvt} + \epsilon_{2\alpha}e^{-iKvt} \mid^2 \times \mathcal{Q}_\beta^\dagger\mathcal{Q}_\alpha\rho_0\mathcal{Q}_\alpha^\dagger\mathcal{Q}_\beta \tag{34}$$

and

$$\mathcal{P}_0 + i\mathcal{S}_0 = \frac{s_0}{2}\left(\frac{\Gamma}{2} + i\Delta\right)\sum_\alpha \mid \epsilon_{1\alpha}e^{iKvt} + \epsilon_{2\alpha}e^{-iKvt} \mid^2 \times \mathcal{Q}_\alpha^\dagger\mathcal{Q}_\alpha, \tag{35}$$

with s_0 the off-resonance saturation parameter

$$s_0 = \frac{\mid \Omega \mid^2/2}{\Delta^2 + \Gamma^2/4}. \tag{36}$$

These expressions demonstrate that the spherical components α of the total field contribute to the evolution in an additive way, and that the phase relation between these components is immaterial in the present case of nearly zero velocity. The time dependence of the evolution operator arises from the time dependence of each separate spherical component. If ρ_0 is diagonal in M at the initial time zero, it will remain diagonal at all times. Furthermore, the steady-state solution of (33) is diagonal, so that ρ_0 and σ_{gg} are identical. This implies that only the diagonal parts of the contributions (17) and (18) to the force operator (16) contribute to the average force. This average force can be written as

$$F_0(t) = \mathrm{Tr}[\rho_0(t)\mathcal{F}_0(t)] \tag{37}$$

with

$$\mathcal{F}_0 = \mathcal{F}_{0,\mathrm{red}} + \mathcal{F}_{0,\mathrm{sc}}. \tag{38}$$

If we substitute (23) and (24) into Eqs. (17) and (18), and retain only the diagonal parts, we arrive at explicit expressions for the redistributive and the scattering part of the force operator. We find

$$\mathcal{F}_{0,\mathrm{red}} = if_{\mathrm{red}}\sum_\alpha(\epsilon_{1\alpha}^*\epsilon_{2\alpha}e^{-2iKvt} - \epsilon_{2\alpha}^*\epsilon_{1\alpha}e^{2iKvt})\mathcal{Q}_\alpha^\dagger\mathcal{Q}_\alpha \tag{39}$$

and

$$\mathcal{F}_{0,\mathrm{sc}} = f_{\mathrm{sc}}\sum_\alpha(\mid \epsilon_{1\alpha} \mid^2 - \mid \epsilon_{2\alpha} \mid^2)\mathcal{Q}_\alpha^\dagger\mathcal{Q}_\alpha. \tag{40}$$

Here we introduced

$$f_{\mathrm{sc}}(\Delta,\Omega) = \hbar K s_0\Gamma/2 \tag{41}$$

and

$$f_{\mathrm{red}}(\Delta,\Omega) = \hbar K s_0\Delta, \tag{42}$$

which represent, respectively, the radiation pressure and the dipole force in the case of a two-level atom in a nonsaturating traveling wave.

In the special case of a standing wave, where $\epsilon_1 = \epsilon_2 = \epsilon$, the operator (40) disappears, so that the force is purely redistributive. We obtain from (39)

$$\mathcal{F}_{0,\mathrm{red}} = 2f_{\mathrm{red}}\sin(2Kvt)\sum_\alpha \mid \epsilon_\alpha \mid^2 \mathcal{Q}_\alpha^\dagger\mathcal{Q}_\alpha. \tag{43}$$

However, it is obvious from (33)–(35) that the entire evolution expressed on the right-hand side of (33) is proportional to $\cos^2(Kvt)$. This implies that the steady-state solution of (33) is independent of time. Hence the expectation value of the force near zero velocity vanishes after averaging over a wavelength in the case of a standing wave.

We emphasize that these expressions for the force operator near zero velocity are independent of the value of the magnetic field. The dependence of the force on **B** arises purely through the density matrix and is illustrated in several plots below. **B** should only be strong enough so that the inequality (20) is justified.

2. $n = 1$: $Kv \cong \omega_Z/2$

Now we turn to the resonance at the velocity obeying the condition

$$\mid 2Kv - \omega_Z \mid \ll \omega_Z. \tag{44}$$

We eliminate the strong Zeeman term in the evolution equation by a transformation to a frame rotating about the magnetic field, and we introduce the density matrix

$$\rho_1(t) = \exp[2iKvJ_gZt/\hbar]\sigma_{gg}(t)\exp[-2iKvJ_gZt/\hbar]. \tag{45}$$

Equations (8)–(10) determine the evolution of ρ_1. Again the rapid oscillations in the evolution operator can be neglected. If we expand the operators $\mathcal{R}$ in (9) and (10) as a sum over $\mathcal{R}_1$ and $\mathcal{R}_2$, and substitute (27) and (29), we only have to keep the terms where the oscillation due to the operators $\exp[\pm 2iKvJ_gZt/\hbar]$ is compensated by the plane-wave factors. The terms containing products of $\mathcal{Q}_\alpha$ and $\mathcal{Q}_{\alpha'}^\dagger$ arising from the same traveling wave survive only if $\alpha = \alpha'$. If $\mathcal{Q}_\alpha$ arises from beam 1, and $\mathcal{Q}_{\alpha'}^\dagger$ from beam 2, the rapid oscillations disappear only in the case that $\alpha' = \alpha + 1$. These terms correspond to Raman-type couplings between Zeeman substates that are Doppler shifted into resonance for the velocity group under consideration. We arrive at the evolution equation

$$\frac{d}{dt}\rho_1(t) = -\frac{i}{\hbar}(\omega_Z - 2Kv)[J_gZ, \rho_1(t)] + \mathcal{G}_1\rho_1(t) - [\mathcal{P}_1 + i\mathcal{S}_1]\rho_1(t) - \rho_1(t)[\mathcal{P}_1 - i\mathcal{S}_1], \tag{46}$$

with

$$\mathcal{G}_1\rho_1 = \frac{s_0\Gamma}{2}\sum_\alpha\sum_\beta\left[(\mid \epsilon_{1\alpha} \mid^2 + \mid \epsilon_{2\alpha} \mid^2)\mathcal{Q}_\beta^\dagger\mathcal{Q}_\alpha\rho_1\mathcal{Q}_\alpha^\dagger\mathcal{Q}_\beta + \epsilon_{1\alpha}\epsilon_{2\,\alpha+1}^*\mathcal{Q}_\beta^\dagger\mathcal{Q}_\alpha\rho_1\mathcal{Q}_{\alpha+1}^\dagger\mathcal{Q}_\beta + \epsilon_{2\,\alpha+1}\epsilon_{1\alpha}^*\mathcal{Q}_\beta^\dagger\mathcal{Q}_{\alpha+1}\rho_1\mathcal{Q}_\alpha^\dagger\mathcal{Q}_\beta\right] \tag{47}$$

and

$$\mathcal{P}_1 + i\mathcal{S}_1 = \frac{s_0}{2}\left(\frac{\Gamma}{2} + i\Delta\right)\sum_{\alpha}\left[(\mid \epsilon_{1\alpha} \mid^2 + \mid \epsilon_{2\alpha} \mid^2)\mathcal{Q}_\alpha^\dagger \mathcal{Q}_\alpha + \epsilon_{1\alpha}\epsilon_{2\,\alpha+1}^* \mathcal{Q}_{\alpha+1}^\dagger \mathcal{Q}_\alpha + \epsilon_{2\,\alpha+1}\epsilon_{1\alpha}^* \mathcal{Q}_\alpha^\dagger \mathcal{Q}_{\alpha+1}\right]. \quad (48)$$

Note that these operators $\mathcal{G}_1, \mathcal{P}_1$, and $\mathcal{S}_1$ do not depend on time. Thus the density matrix ρ_1 is also independent of time in the steady state. On the other hand, this steady-state solution does depend on the velocity component of v parallel to $\mathbf{K}$. Off-diagonal matrix elements between the Zeeman substates arise from the terms in (47) and (48) that contain mixed products of components of both polarization vectors. They represent the resonant Raman-type couplings.

A corresponding transformation must be performed on the force operators, in order that the average force is determined by

$$F_1(t) = \mathrm{Tr}[\rho_1(t)(\mathcal{F}_{1,\mathrm{red}} + \mathcal{F}_{1,\mathrm{sc}})]. \quad (49)$$

It is noteworthy that the resonance in the force, which derives from the density matrix and not from the operator, simply displaces with the resonant velocity $v = \omega_Z/2K$ when the magnetic field strength is varied [14]. Ignoring rapid oscillations, we arrive at the expressions

$$\mathcal{F}_{1,\mathrm{red}} = if_{\mathrm{red}}\sum_{\alpha}[\,\epsilon_{1\alpha}^*\epsilon_{2\,\alpha+1}\mathcal{Q}_\alpha^\dagger \mathcal{Q}_{\alpha+1} - \epsilon_{2\,\alpha+1}^*\epsilon_{1\alpha}\mathcal{Q}_{\alpha+1}^\dagger \mathcal{Q}_\alpha] \quad (50)$$

and

$$\mathcal{F}_{1,\mathrm{sc}} = f_{\mathrm{sc}}\sum_{\alpha}(\mid \epsilon_{1\alpha} \mid^2 - \mid \epsilon_{2\alpha} \mid^2)\mathcal{Q}_\alpha^\dagger \mathcal{Q}_\alpha. \quad (51)$$

The operator (50) for the redistributive force is determined by the difference in the transfer of photons from beam 1 to beam 2 and *vice versa*. The scattering-force operator (51) is identical to the scattering force $\mathcal{F}_{0,\mathrm{sc}}$ near zero velocity, and it disappears for a standing wave. The redistributive force only probes the coherences between the Zeeman substates with $\Delta M = \pm 1$.

3. $n = 2$: $Kv \cong \omega_Z$

Finally we treat the resonance at the velocity given by the condition $\mid 2Kv - 2\omega_Z \mid << \omega_Z$, and we follow a similar method as in previous cases. The dominant part of the Larmor precession is eliminated by the transformation

$$\rho_2(t) = \exp[iKvJ_{gZ}t/\hbar]\sigma_{gg}(t)\exp[-iKvJ_{gZ}t/\hbar]. \quad (52)$$

Then only a weak precession term remains. In the evolution equation for ρ_2 we neglect the rapidly oscillating terms. Now only the Raman-type couplings between Zeeman sublevels with $\Delta m = \pm 2$ survive, which are resonant for the present velocity class. The effective evolution equation takes the form

$$\frac{d}{dt}\rho_2(t) = -\frac{i}{\hbar}(\omega_Z - Kv)[J_{gZ}, \rho_2(t)] + \mathcal{G}_2\rho_2(t) - [\mathcal{P}_2 + i\mathcal{S}_2]\rho_2(t) - \rho_2(t)[\mathcal{P}_2 - i\mathcal{S}_2], \quad (53)$$

with

$$\mathcal{G}_2\rho_2 = \frac{s_0\Gamma}{2}\sum_{\alpha}\sum_{\beta}\left[(\mid \epsilon_{1\alpha} \mid^2 + \mid \epsilon_{2\alpha} \mid^2)\mathcal{Q}_\beta^\dagger \mathcal{Q}_\alpha \rho_2 \mathcal{Q}_\alpha^\dagger \mathcal{Q}_\beta + \epsilon_{1\alpha}\epsilon_{2\,\alpha+2}^* \mathcal{Q}_\beta^\dagger \mathcal{Q}_\alpha \rho_2 \mathcal{Q}_{\alpha+2}^\dagger \mathcal{Q}_\beta + \epsilon_{2\,\alpha+2}\epsilon_{1\alpha}^* \mathcal{Q}_\beta^\dagger \mathcal{Q}_{\alpha+2}\rho_2 \mathcal{Q}_\alpha^\dagger \mathcal{Q}_\beta\right] \quad (54)$$

and

$$\mathcal{P}_2 + i\mathcal{S}_2 = \frac{s_0}{2}\left(\frac{\Gamma}{2} + i\Delta\right)\sum_{\alpha}\left[(\mid \epsilon_{1\alpha} \mid^2 + \mid \epsilon_{2\alpha} \mid^2)\mathcal{Q}_\alpha^\dagger \mathcal{Q}_\alpha + \epsilon_{1\alpha}\epsilon_{2\,\alpha+2}^* \mathcal{Q}_{\alpha+2}^\dagger \mathcal{Q}_\alpha + \epsilon_{2\,\alpha+2}\epsilon_{1\alpha}^* \mathcal{Q}_\alpha^\dagger \mathcal{Q}_{\alpha+2}\right]. \quad (55)$$

Obviously, since α can only attain the values $-1, 0, 1$, in the last terms of (54) and (55), which contain products of spherical components of the two polarization vectors, only the summand with $\alpha = -1$ contributes. The force near $v \cong \omega_Z/K$ is expressed as

$$F_2(t) = \mathrm{Tr}[\rho_2(t)(\mathcal{F}_{2,\mathrm{red}} + \mathcal{F}_{2,\mathrm{sc}})], \quad (56)$$

with

$$\mathcal{F}_{2,\mathrm{red}} = if_{\mathrm{red}}\sum_{\alpha}[\,\epsilon_{1\alpha}^*\epsilon_{2\,\alpha+2}\mathcal{Q}_\alpha^\dagger \mathcal{Q}_{\alpha+2} - \epsilon_{2\,\alpha+2}^*\epsilon_{1\alpha}\mathcal{Q}_{\alpha+2}^\dagger \mathcal{Q}_\alpha] \quad (57)$$

and

$$\mathcal{F}_{2,\mathrm{sc}} = f_{\mathrm{sc}}\sum_{\alpha}(\mid \epsilon_{1\alpha} \mid^2 - \mid \epsilon_{2\alpha} \mid^2)\mathcal{Q}_\alpha^\dagger \mathcal{Q}_\alpha. \quad (58)$$

In Eq. (57) for the redistributive force, only the term with $\alpha = -1$ contributes. We only kept the present form in order to stress the analogy with Eq. (50). The redistributive force probes the Zeeman coherence with $\Delta M = \pm 2$, and can therefore only arise when $J_g \geq 1$. Furthermore, it is only sensitive to the polarization components normal to the magnetic field. The scattering force operator is given by the same expression as for the other resonances. Therefore the scattering force is zero for a standing wave.

The results of this subsection demonstrate that the

magnetic field has no effect on the force operators, and that its sole effect is to determine the resonance velocity in the density matrix. The width of the resonances is independent of the magnetic field, and it is determined by the pump rate and the light shift in the same way as in the case of polarization gradient cooling in the absence of a magnetic field. Roughly, this velocity width of the resonances is of the order of $\Delta v \propto s_0\Gamma/K$ [2].

D. Transverse field

First we consider the situation of a transverse magnetic field. With the Z axis chosen along the field, we select the X axis along the propagation direction of the laser beams as shown in Figs. 3 and 4. Since the two polarization vectors can have no X component, we obtain from (28)

$$\epsilon_{i1} = \epsilon_{i-1} = i\epsilon_{iY}/\sqrt{2} \quad , \quad \epsilon_{i0} = \epsilon_{iZ}. \tag{59}$$

Hence the two circular components of each polarization are equal. Moreover, since the polarization vectors ϵ_1 and ϵ_2 are normalized, we know that

$$|\,\epsilon_{iY}\,|^2 = 1 - |\,\epsilon_{iZ}\,|^2, \tag{60}$$

for $i = 1,2$.

According to (40), (51), and (58), the scattering force operator is given by the same expression in all velocity-selective resonances. For a transverse field, Eqs. (59) and (60) can be used to demonstrate that this operator can be expressed as

$$\mathcal{F}_{0,\mathrm{sc}} = \mathcal{F}_{1,\mathrm{sc}} = \mathcal{F}_{2,\mathrm{sc}} = f_{\mathrm{sc}}(|\,\epsilon_{1Z}\,|^2 - |\,\epsilon_{2Z}\,|^2)\mathcal{A} \tag{61}$$

in terms of the operator

$$\mathcal{A} = \mathcal{Q}_0^\dagger\mathcal{Q}_0 - \tfrac{1}{2}(\mathcal{Q}_1^\dagger\mathcal{Q}_1 + \mathcal{Q}_{-1}^\dagger\mathcal{Q}_{-1}). \tag{62}$$

Apart from a constant factor, the expectation value of $\mathcal{A}$ is the ZZ component of the alignment tensor of the ground state, or, equivalently, the multipole component T_{kq} with $k = 2, q = 0$. Since the ground state can only have alignment when $J_g \geq 1$, the scattering force must disappear for $J_g = 1/2$.

Substitution of (59) and (60) in the expressions (39), (50), and (57) for the redistributive force operators leads to the simplified forms in the present case of a transverse magnetic field

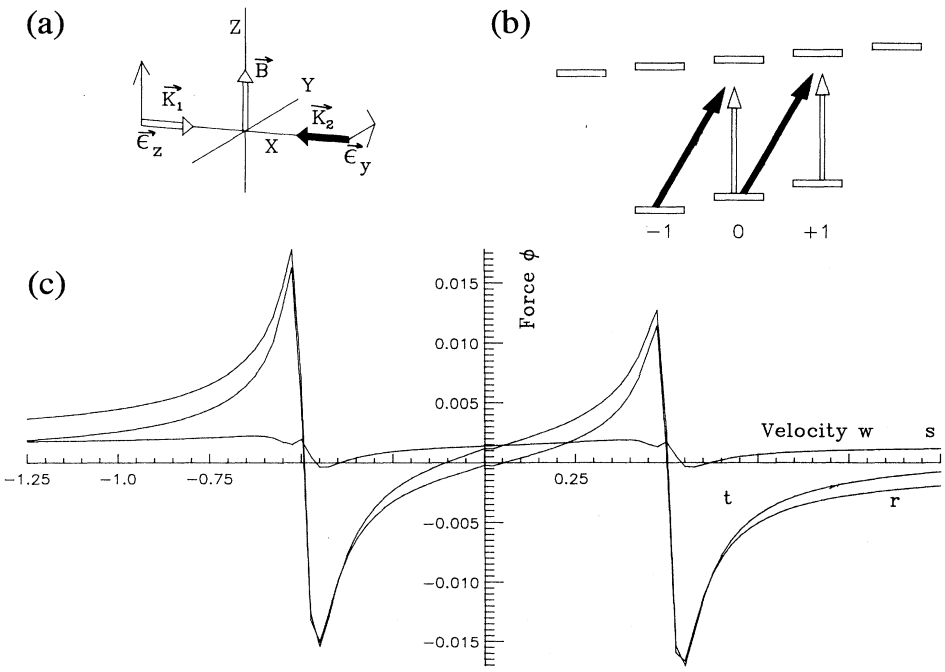

FIG. 3. The reduced force ϕ on atoms in units of $\hbar K\Omega^2/\Gamma$ as a function of the reduced velocity w in units of $\Omega^2/K\Gamma$ for the lin $\perp$ lin case with a transverse magnetic field $\mathbf{B} = B\hat{\mathbf{z}}$ for a $J_g = 1$ to $J_e = 2$ transition. The reduced strength of the magnetic field $b = \omega_Z\Gamma/\Omega^2 = 1$ and the detuning of the laser $\Delta = -1.5\Gamma$. (a) The geometry of the laser beams and magnetic field. (b) The level scheme with the transitions that form the VSR for $v_r = +\omega_Z/2K$ $(n = 1)$. The transitions indicated with a solid arrow are induced by the light beam propagating against the atomic velocity and the transitions indicated with an open arrow are induced by the light beam copropagating with the atomic velocity. Since the counterpropagating beam has a polarization vector perpendicular to the magnetic field, it can induce both σ_+ and σ_- transitions in a quantization frame parallel to $\mathbf{B}$. Note that only those transitions that form the $(n = 1)$ resonance are indicated. (c) The result of numerical calculation of the force as a function of velocity. The different components of the force are indicated by the letters s for scattering, r for redistribution, and t for total force.

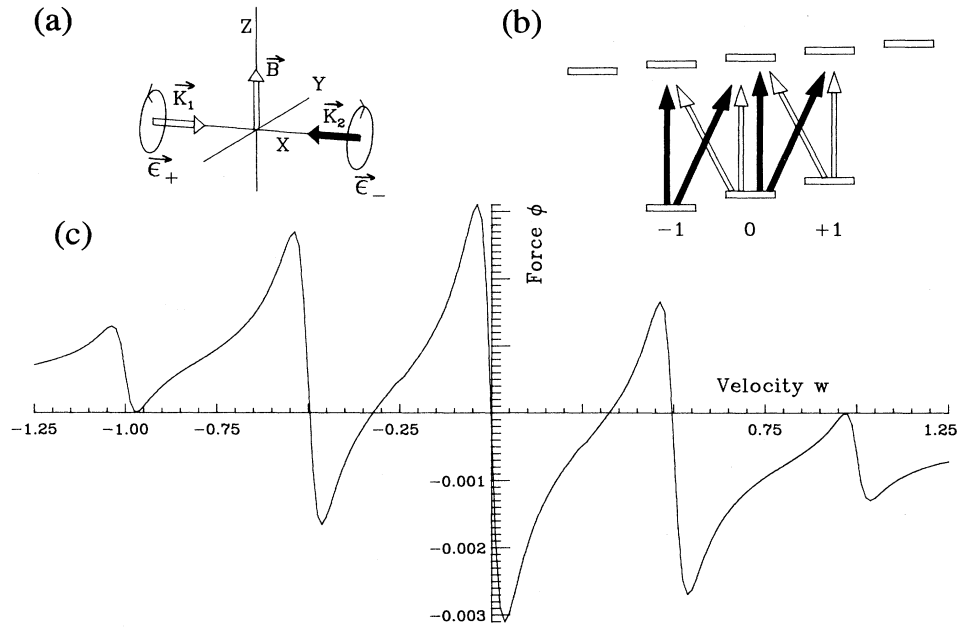

FIG. 4. The reduced force ϕ on atoms as a function of the reduced velocity w for the $\sigma_+ - \sigma_-$ case with a transverse magnetic field $\mathbf{B} = B\hat{\mathbf{z}}$ for a $J_g = 1$ to $J_e = 2$ transition (see also Fig. 3). The transitions shown in (b) form the VSR for $v_r = +\omega_Z/2K$ $(n = 1)$. Since both circular polarizations have components parallel and perpendicular to $\mathbf{B}$, each light beam can induce σ_+, σ_-, and π transitions. The calculations show that all the resonances $(n = 0, \pm 1, \pm 2)$ are present in this case as explained in the text. The reduced magnetic field strength $b = 1$ and the laser detuning $\Delta = -1.5\Gamma$. For the definition of b, ϕ, and w see the caption of Fig. 3.

$$\mathcal{F}_{0,\mathrm{red}} = if_{\mathrm{red}}[\,(\epsilon_{1Z}^*\epsilon_{2Z}e^{-2iKvt} - \epsilon_{2Z}^*\epsilon_{1Z}e^{2iKvt})\mathcal{Q}_0^\dagger\mathcal{Q}_0 + \tfrac{1}{2}(\epsilon_{1Y}^*\epsilon_{2Y}e^{-2iKvt} - \epsilon_{2Y}^*\epsilon_{1Y}e^{2iKvt}) \times(\mathcal{Q}_1^\dagger\mathcal{Q}_1 + \mathcal{Q}_{-1}^\dagger\mathcal{Q}_{-1})], \tag{63}$$

$$\mathcal{F}_{1,\mathrm{red}} = if_{\mathrm{red}}[\,\epsilon_{1Z}^* i\epsilon_{2Y}\mathcal{Q}_0^\dagger\mathcal{Q}_1/\sqrt{2} - i\epsilon_{1Y}^*\epsilon_{2Z}\mathcal{Q}_{-1}^\dagger\mathcal{Q}_0/\sqrt{2} - \epsilon_{2Z}^* i\epsilon_{1Y}\mathcal{Q}_0^\dagger\mathcal{Q}_{-1}/\sqrt{2} + i\epsilon_{2Y}^*\epsilon_{1Z}\mathcal{Q}_1^\dagger\mathcal{Q}_0/\sqrt{2}], \tag{64}$$

$$\mathcal{F}_{2,\mathrm{red}} = if_{\mathrm{red}}\left[\epsilon_{1Y}^*\epsilon_{2Y}\mathcal{Q}_{-1}^\dagger\mathcal{Q}_1/2 - \epsilon_{2Y}^*\epsilon_{1Y}\mathcal{Q}_1^\dagger\mathcal{Q}_{-1}/2\right]. \tag{65}$$

Obviously, $\mathcal{F}_{1,\mathrm{red}}$ is determined by the Z component of the field of one beam, and the Y component of the field of the other beam. $\mathcal{F}_{2,\mathrm{red}}$ depends only on the Y components of both traveling waves. This is understandable from the picture of the velocity-selective resonances, as illustrated in Fig. 3(b).

When the two polarization vectors are orthogonal, they obey in addition to the normalization condition (60) the orthogonality relation

$$\epsilon_{1Z}^*\epsilon_{2Z} = -\epsilon_{1Y}^*\epsilon_{2Y}. \tag{66}$$

If we substitute this relation in Eq. (63) for $\mathcal{F}_{0,\mathrm{red}}$, we obtain the result

$$\mathcal{F}_{0,\mathrm{red}} = if_{\mathrm{red}}\left(\epsilon_{1Z}^*\epsilon_{2Z}e^{-2iKvt} - \epsilon_{2Z}^*\epsilon_{1Z}e^{2iKvt}\right)\mathcal{A}, \tag{67}$$

so that it probes the alignment of the ground state, just as the scattering force. Since the phase relation between the Z component and the Y component of the field is irrelevant, the resulting force near zero velocity is the same in the cases $\boldsymbol{\epsilon}_1 = (\hat{\mathbf{Y}} + i\hat{\mathbf{Z}})/\sqrt{2}$, $\boldsymbol{\epsilon}_2 = (\hat{\mathbf{Y}} - i\hat{\mathbf{Z}})/\sqrt{2}$ (opposite circular polarizations, $\sigma_+ - \sigma_-$) and $\boldsymbol{\epsilon}_1 = (\hat{\mathbf{Y}} + \hat{\mathbf{Z}})/\sqrt{2}$, $\boldsymbol{\epsilon}_2 = (\Phi\hat{\mathbf{Y}} - \hat{\mathbf{Z}})/\sqrt{2}$ (orthogonal linear polarizations lin $\perp$ lin with the same magnitude of optical electric field parallel to the $\mathbf{B}$ field). In these cases, the Y component and the Z component of the field constitute two standing waves with the locations of the nodes and the antinodes interchanged. The scattering force $\mathcal{F}_{0,\mathrm{sc}}$ disappears in these cases, and the force is purely redistributive.

The conclusions are summarized on the left side of Table I, which shows when the force operator vanishes for the different resonances $(n = 0, \pm 1, \pm 2)$ in the case of a standing wave of constant polarization or in the case of orthogonal polarization (polarization gradient). For those cases where the force operator does not vanish, Table I shows schematically how the resonance depends on the components of the polarization vector along the Z and Y axes.

To illustrate the case of transverse magnetic field two examples are given in Figs. 3 and 4 where we show numerical calculations for the force with the procedure as outlined in [11]. The method relies on calculating the density matrix by expansion of its elements in a Fourier series. The resulting set of coupled linear relations between the Fourier coefficients is then solved numerically as a function of velocity. In Fig. 3 we have chosen one of the polarizations along the magnetic field ($\boldsymbol{\epsilon}_1 = \hat{\mathbf{Z}}$) and

the other perpendicular to the magnetic field ($\epsilon_2 = \hat{\mathbf{Y}}$). From Table I we can infer that in this case only the ($n = \pm 1$) resonances for the redistribution force will remain. In Fig. 4 we have chosen circular polarization and each light beam now contains both Z and Y components. In that case all resonances remain, as can be seen in Fig. 4.

E. Longitudinal field

Next, we consider the case of two counterpropagating plane waves of equal intensity in the presence of a strong longitudinal magnetic field. This implies that the propagation direction of the beams coincides with the magnetic field, which is the Z axis, as shown in Fig. 5. We decompose the polarization vectors in their circular components as

$$\boldsymbol{\epsilon}_i = \epsilon_{i+}\mathbf{u}_1 + \epsilon_{i-}\mathbf{u}_{-1}, \tag{68}$$

for $i = 1, 2$. The polarizations have no component along the magnetic field, and the radiation fields induce no π transitions. Therefore, the operators $\mathcal{P}$ and $\mathcal{S}$ in (8) cannot couple Zeeman substates $\mid M\rangle$ and $\mid M'\rangle$ with $M' - M = 1$. This means that the Zeeman resonances predicted by (25) for $n = \pm 1$ are absent for a longitudinal field.

The resonance near $v = 0$ is described by the evolution

TABLE I. Summary of the results obtained in Sec. II. Each cell entry in the table indicates in order: (1) The value of the angular momentum J_g for which the VSR resonance occurs, (2) if the resonance depends on the alignment $\mathcal{A}$ of the ground state, (3) the dependence of the resonance on the polarization components of the two beams (i, j)=(1,2), (4) the equation number with the force operator for this particular resonance, and (5) the figure with the calculation of an example for which this resonance is present. A single zero indicates when the force becomes zero, which is if either the force operator is zero or when the force becomes zero after averaging over a wavelength.

			Trans. magn. field $\mathbf{B} \perp \mathbf{K}$		Long. magn. field $\mathbf{B} \parallel \mathbf{K}$		
			stand. wave	orthog. pol.	stand. wave	orthog. pol.	
n	v_r	Force	$\epsilon_1 = \epsilon_2$	$\epsilon_1 \perp \epsilon_2$	$\epsilon_1 = \epsilon_2$	lin $\perp$ lin	$\sigma_+ - \sigma_-$
0	0	$F_{0,\mathrm{sc}}$	0	$J_g \geq 1$ $\propto \mathcal{A}$ $\mid \epsilon_{iZ} \mid^2$ Eq. (60) –	0	0	0
		$F_{0,\mathrm{red}}$	0	$J_g \geq 1$ $\propto \mathcal{A}$ $\epsilon_{iZ}\epsilon^*_{jZ}$ Eq. (66) Figs. 2,5	0	$J_g \geq 1/2$ $\epsilon_{i\pm}\epsilon^*_{j\pm}$ Eq. (68)	0
± 1	$\pm\frac{\omega_L}{2K}$	$F_{1,\mathrm{sc}}$	0	$J_g \geq 1$ $\propto \mathcal{A}$ $\mid \epsilon_{iZ} \mid^2$ Eq. (60) Fig. 1	0	0	0
		$F_{1,\mathrm{red}}$	$J_g \geq 1/2$ – $\epsilon_{iZ}\epsilon^*_{jY}$ Eq. (63) Fig. 4	$J_g \geq 1/2$ – $\epsilon_{iZ}\epsilon^*_{jY}$ Eq. (63) Figs. 1,2	0	0	0
± 2	$\pm\frac{\omega_L}{K}$	$F_{2,\mathrm{sc}}$	0	$J_g \geq 1$ $\propto \mathcal{A}$ $\mid \epsilon_{iZ} \mid^2$ Eq. (60)	0	0	$J_g \geq 1$ $\mid \epsilon_{i\pm} \mid^2$ Eq. (69) Fig. 3
		$F_{2,\mathrm{red}}$	$J_g \geq 1$ – $\epsilon_{iY}\epsilon^*_{jY}$ Eq. (64)	$J_g \geq 1$ – $\epsilon_{iY}\epsilon^*_{jY}$ Eq. (64) Fig. 2	$J_g \geq 1$ – $\epsilon_{i\mp}\epsilon^*_{j\pm}$ Eq. (64)	$J_g \geq 1$ – $\epsilon_{i\mp}\epsilon^*_{j\pm}$ Eq. (64)	$J_g \geq 1$ – $\epsilon_{i\mp}\epsilon^*_{j\pm}$ Eq. (64) Fig. 3

equation (33), where now the expressions for the operators $\mathcal{G}_0, \mathcal{P}_0$, and $\mathcal{S}_0$ contain only contributions from $\mathcal{Q}_1$ and $\mathcal{Q}_{-1}$. The force operators $\mathcal{F}_{0,\mathrm{red}}$ and $\mathcal{F}_{0,\mathrm{sc}}$ as given by (39) and (40) now take the form

$$\mathcal{F}_{0,\mathrm{red}} = if_{\mathrm{red}}[(\epsilon_{1+}^{*}\epsilon_{2+}e^{-2iKvt} - \epsilon_{2+}^{*}\epsilon_{1+}e^{2iKvt})\mathcal{Q}_1^{\dagger}\mathcal{Q}_1 + (\epsilon_{1-}^{*}\epsilon_{2-}e^{-2iKvt} - \epsilon_{2-}^{*}\epsilon_{1-}e^{2iKvt})\mathcal{Q}_{-1}^{\dagger}\mathcal{Q}_{-1}] \tag{69}$$

and

$$\mathcal{F}_{0,\mathrm{sc}} = f_{\mathrm{sc}}[(|\epsilon_{1+}|^2 - |\epsilon_{2+}|^2)\mathcal{Q}_1^{\dagger}\mathcal{Q}_1 + (|\epsilon_{1-}|^2 - |\epsilon_{2-}|^2)\mathcal{Q}_{-1}^{\dagger}\mathcal{Q}_{-1}]. \tag{70}$$

For linear polarizations, all circular components $\epsilon_{i\alpha}$ for $\alpha = \pm 1$ have equal strength, and the scattering force $\mathcal{F}_{0,\mathrm{sc}}$ near zero velocity vanishes. On the other hand, for two opposite circular polarizations, the operator $\mathcal{F}_{0,\mathrm{red}}$ is zero. However, in this case the evolution of ρ_0 is simply the incoherent combination of a right-hand and a left-hand circularly polarized pump of equal strength. Then the average force F_0 vanishes completely, as follows directly from symmetry considerations. This we shall discuss below.

For $n = 1$ the force near $Kv = \omega_Z/2$ vanishes as above, and for $n = 2$ the force near $Kv = \omega_Z$ is described by the effective density matrix ρ_2, which obeys the evolution equation (53). The operator for the redistributive force as given by (57) now takes the form

$$\mathcal{F}_{2,\mathrm{red}} = if_{\mathrm{red}}\left[\epsilon_{1-}^{*}\epsilon_{2+}\mathcal{Q}_{-1}^{\dagger}\mathcal{Q}_1 - \epsilon_{2+}^{*}\epsilon_{1-}\mathcal{Q}_1^{\dagger}\mathcal{Q}_{-1}\right], \tag{71}$$

whereas $\mathcal{F}_{2,\mathrm{sc}}$ is equal to $\mathcal{F}_{0,\mathrm{sc}}$.

The results for a longitudinal field are summarized on the right side of Table I, which shows the conditions where resonances can be observed in the cases of a standing wave of constant polarization, of orthogonal linear polarization (lin $\perp$ lin), and of orthogonal circular polarization ($\sigma_+ - \sigma_-$). As the table shows, most resonances vanish for longitudinal magnetic field.

We turn to the explicit case of opposite circular polarizations, where $\boldsymbol{\epsilon}_1 = \mathbf{u}_{-1}$ and $\boldsymbol{\epsilon}_2 = \mathbf{u}_1$. The radiation field takes the form of a helix of linear polarizations [15]. Then the effect of the motion of the atom on its evolution is identical to the effect of a longitudinal magnetic field [2, 10]. An atom moving with velocity v experiences a rotation of the linear polarization with angular velocity Kv. This rotation can be compensated by an additional magnetic field in the Z direction, leading to a Larmor precession frequency $\omega_Z = \mathbf{K}\cdot\mathbf{v}$. The evolution of the atom with velocity v in this additional field is thus the same as for an atom at rest without this field. This can be demonstrated explicitly by considering the corotating density matrix $\rho_2(t)$, as defined in (52). It is easily checked that the effective evolution operators $\mathcal{G}_2$, $\mathcal{P}_2$, and $\mathcal{S}_2$ in the present case of $\sigma_- - \sigma_+$ polarizations are exactly equal to the operators $\mathcal{G}$, $\mathcal{P}$, and $\mathcal{S}$, defined in (9) and (10), at time zero. Hence the velocity-induced time

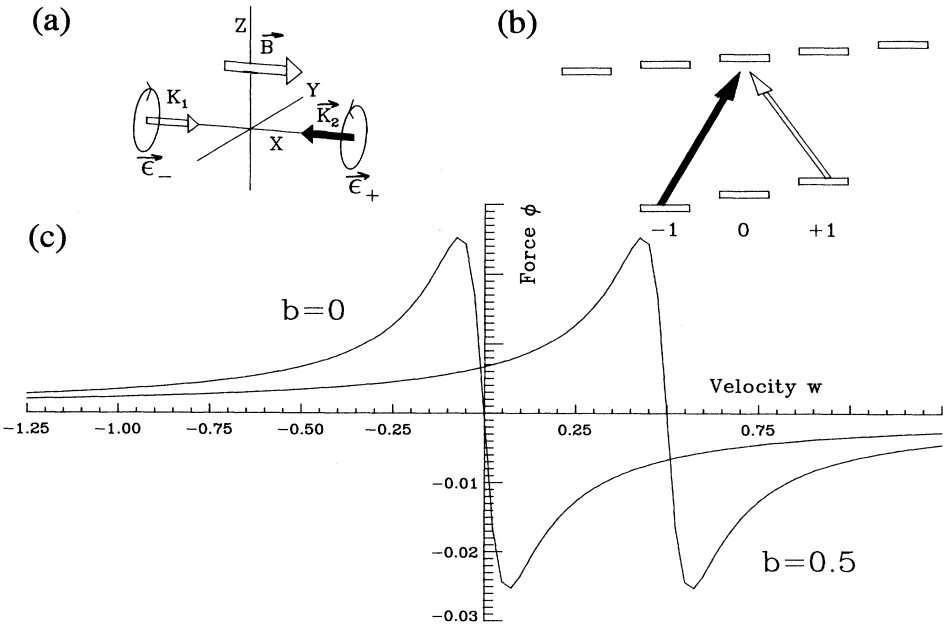

FIG. 5. The reduced force ϕ on atoms as a function of the reduced velocity w for the $\sigma_+ - \sigma_-$ case with a longitudinal magnetic field $\mathbf{B} = B\hat{\mathbf{z}}$ for a $J_g = 1$ to $J_e = 2$ transition. As can be seen in (b) two states with $\Delta M = M_g - M_g'$ can be coupled by VSR, if and only if $\Delta M = 2$ ($n = 2$). The calculations shown are for a reduced field $b = 0$ and $b = 1$. As explained in the text, changing the magnetic field only shifts the resonance [14] according to the VSR condition $v_r = \omega_Z/K$ for ($n = 2$). For the definition of b, ϕ, and w see the caption of Fig. 3.

dependence of these operators is eliminated by the transformation (52) to a rotating frame. The Coriolis forces resulting from this transformation are expressed by the term $\mathbf{K}\cdot\mathbf{v}$ that is subtracted from the Larmor frequency ω_Z in (53). Hence the time-dependent density matrix ρ_2 for a given velocity v in a magnetic field with Larmor frequency ω_Z is identical to the density matrix σ_{gg} for zero velocity, in the reduced magnetic field with the Larmor frequency $\omega_Z - \mathbf{K}\cdot\mathbf{v}$. For the average force as a function of the velocity and the Larmor frequency we find

$$F(v,\omega_Z) = F(0,\omega_Z - Kv) = F(v-\omega_Z/K,0). \tag{72}$$

This equality shows that the effect of a magnetic field is simply to shift the force as a function of the velocity. In the absence of a magnetic field and for negative values of the detuning Δ, the $\sigma_- - \sigma_+$ configuration leads to cooling to zero velocity. Imposing a magnetic field then leads to cooling to the velocity ω_Z/K [14]. The $v=0$ resonance in the absence of the field is simply shifted, and leads to the resonance indicated by (30) for $n=2$. The other values of n do not lead to resonant behavior in this special case. We have illustrated this example with a numerical calculation of the force in Fig. 5.

F. Examples

We will now turn our attention to a few specific examples with a transverse magnetic field that illustrate the results of Sec. II D. Depending on J_g, J_e, and the laser beam polarizations, we can determine which velocity-selective resonances between Zeeman sublevels of $|\,g\rangle$ can cause force resonances simply by inspection of the force expressions. These predictions will be compared with numerical calculations for the force, which have been outlined in a previous paper [11].

The first example is a $J_g = 1/2 \leftrightarrow J_e = 3/2$ transition in a standing wave with right-hand circularly polarized light [see Fig. 6(a)]. The scattering force, which is described by the operator (61) for all resonances, must be zero, since the ground state can have no alignment. The $(n=0)$ resonance in the redistribution force, which is described by the operator (63), is proportional to the alignment operator $\mathcal{A}$ in the case of a standing wave, so that it also vanishes. In addition, the $(n=\pm 2)$ resonance in the redistribution force must also vanish for the considered transition, as has been explained following Eq. (57). Hence only the redistributive $(n=\pm 1)$ resonances can produce a cooling force on atoms, and we shall explicitly evaluate this force.

The evolution equation is given by (46)–(48), and the force operator by (64). Explicit expressions are obtained if we substitute the polarization components

$$\epsilon_{1Y} = \epsilon_{2Y} = 1/\sqrt{2} \quad , \quad \epsilon_{1Z} = \epsilon_{2Z} = i/\sqrt{2}. \tag{73}$$

We denote the matrix elements of the 2×2 density matrix ρ_1 as ρ_{++}, ρ_{+-}, ρ_{-+}, and ρ_{--} for $\langle 1/2 \pm 1/2 \mid \rho_1 \mid 1/2 \pm 1/2\rangle$. After these substitutions the evolution equation (46) for $n=1$ takes the explicit form

$$\begin{aligned}\frac{d}{dt}\rho_{++} &= \frac{s_0\Gamma}{6}(\rho_{--}-\rho_{++}) + \frac{i\Delta s_0}{6}(\rho_{+-}-\rho_{-+}) \\ &= -\frac{d}{dt}\rho_{--},\end{aligned} \tag{74}$$

$$\begin{aligned}\frac{d}{dt}\rho_{+-} = &-i(\omega_Z - 2Kv)\rho_{+-} - \frac{s_0\Gamma}{18}(5\rho_{+-}-\rho_{++}-\rho_{--}) \\ &+\frac{i\Delta s_0}{3}(\rho_{++}-\rho_{--}),\end{aligned} \tag{75}$$

with $\rho_{+-} = \rho_{-+}^*$, $\rho_{--} = 1-\rho_{++}$. The equation (49) for the average force yields in the present case

$$F_1 = \frac{i}{3} f_{\mathrm{red}}(\rho_{-+}-\rho_{+-}). \tag{76}$$

In the steady state, we obtain as the final result for the force

$$F_1 = \frac{-\beta(v-v_r)}{1+[(v-v_r)/v_c]^2}, \tag{77}$$

where β is the effective velocity damping constant

$$\beta = -\hbar K^2 \frac{24\Delta\Gamma}{25\Gamma^2+30\Delta^2} \tag{78}$$

and the critical velocity v_c is determined by

$$v_c^2 = \left(\frac{s_0}{36K}\right)^2 (25\Gamma^2+30\Delta^2)\,. \tag{79}$$

The resonant velocity is $v_r = \omega_Z/2K$. Cooling to this resonant velocity takes place when β is positive, which is the case for negative values of the detuning Δ.

The shape of the $(n=-1)$ resonance follows from this result (77) if we use parity invariance. Since both the magnetic field and the polarization are invariant for parity transformations, we obtain the identity

$$F(-v) = -F(v), \tag{80}$$

so that F is an odd function of the velocity. It follows that both resonances lead to cooling for negative values of the detuning Δ. The $(n=\pm 1)$ resonances for the force as a function of the velocity have a simple dispersion shape. The critical velocity v_c is proportional to the intensity, but the damping constant β is independent of the intensity. Equation (76) demonstrates that the force is sensitive only to the coherences between the Zeeman sublevels as expected for a redistributive force.

In Fig. 6 we have compared our analytical result from (77) with the result of numerical calculations. The small discrepancies between the analytical and numerical results are caused by the fact that in the numerical calculation we do not impose a limit on the optical pumping rate, as is done in order to obtain the analytical result as indicated in Eq. (20).

Redistributive forces discussed so far were explained in terms of gradients of the light shift [2, 3, 5]. We wish to emphasize, however, that in the present case the light shifts are constant, and a Sisyphus picture does not apply. As indicated by (19), the force can be expressed in terms of the gradient of the light-shift operator. Notice that

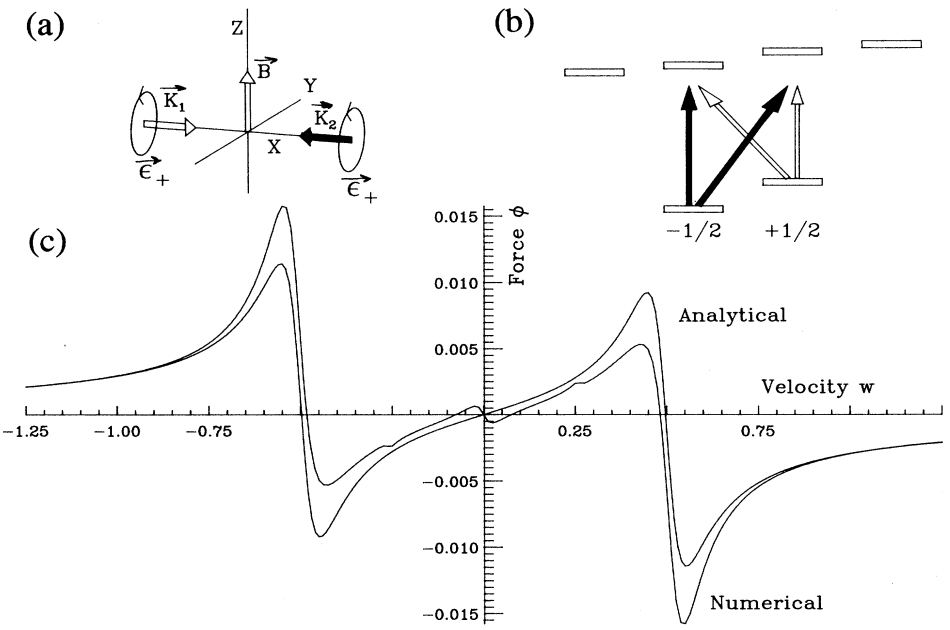

FIG. 6. The reduced force ϕ on atoms as a function of the reduced velocity w for the $\sigma_+ - \sigma_+$ case with a transverse magnetic field $\mathbf{B} = B\hat{\mathbf{z}}$ (MILC) for a $J_g = 1/2$ to $J_e = 3/2$ transition. Since both circular polarizations have components parallel and perpendicular to $\mathbf{B}$, each light beam can induce σ_+, σ_-, and π transitions. In a standing wave the $(n = 0)$ resonance disappears, and since $J_g = 1/2$, the $(n = 2)$ resonance is not present. The analytical calculation for the $(n = \pm 1)$ resonance is compared to numerical calculation for reduced magnetic field $b = 1$ and detuning $\Delta = -1.5\Gamma$. The deviations between the analytical and numerical results are caused by the fact that γ_P cannot completely be neglected compared to ω_Z, as is done in order to obtain the analytical result. For the definition of b, ϕ, and w see the caption of Fig. 3.

the operator $\mathcal{S}_1$ as defined in (48), which is independent of the position, is the light-shift operator in the frame rotating with the angular velocity equal to Kv. Hence the eigenvalues of $\mathcal{S}_1$ are independent of position, and the light-shift gradients are zero. But the corresponding eigenstates perform a full rotation over 2π when the atom traverses half a wavelength. This implies that we have encountered a redistributive force which results from the position dependence of the eigenstates of $\mathcal{S}_1$, while the light shifts themselves do not vary with position. At the nodes and at the antinodes of the standing wave, the eigenstates of $\mathcal{S}_1$ are the eigenstates of J_{gX}. Note, the same force has been encountered before in Ref. [2], in which case it represented a small part of the force for the $\sigma_+ - \sigma_-$ configuration, whereas the main part of the force consisted of a scattering force. In this case the force is totally redistributive.

As a second example we consider the $(n = 0)$ resonance for a transition with $J_g = 1$, $J_e = 0$, in two counter-propagating waves with orthogonal linear polarizations at angles of $\pm 45°$ with the magnetic field (see Fig. 7). Thus

$$\epsilon_{1Y} = \epsilon_{2Y} = 1/\sqrt{2} \quad , \quad \epsilon_{1Z} = -\epsilon_{2Z} = 1/\sqrt{2}. \tag{81}$$

The evolution equations of the density matrix ρ_0 only couple the diagonal elements amongst themselves, and we can restrict our discussion to the populations of the three Zeeman sublevels. We denote these populations as a_M, for $M = -1, 0, 1$. The three Clebsch-Gordan coefficients are all equal to $1/\sqrt{3}$. From Eqs. (33)–(35) we obtain the evolution equations for these populations. Since the coupling of the two states with $M = \pm 1$ to the excited state are equal, the populations a_1 and a_{-1} are identical. Because of normalization, we obtain an evolution equation for a_0 alone, which can be put in the form

$$\frac{d}{dt}a_0 = \frac{s_0\Gamma}{18}\{\cos^2(Kvt) - [4 - 3\cos^2(Kvt)]a_0\}. \tag{82}$$

The scattering force disappears according to (61), since the Z components of both fields have the same strength. The operator for the redistribution force is given in (63). For the present configuration, its expectation value is

$$F_0 = -\tfrac{1}{2} f_{\text{red}} \sin(2Kvt)(a_0 - \tfrac{1}{3}). \tag{83}$$

A full analytical expression for a_0 is not easily obtainable, and we restrict ourselves to an expression linear in the velocity. In the steady state and for a given velocity v we obtain the explicit expression for the population of the state $M = 0$ as a function of the position X along the beams

$$a_0(X) = \frac{\cos^2(KX)}{4 - 3\cos^2(KX)} + \left(\frac{144Kv}{s_0\Gamma}\right)\frac{\cos(KX)\sin(KX)}{[4 - 3\cos^2(KX)]^3}. \tag{84}$$

The average force is now obtained if we substitute this result in (83), and take the average over a wavelength. The resulting integral can be performed analytically if we take $[4 - 3\cos^2(KX)]^{-1}$ as a new integration variable. We find

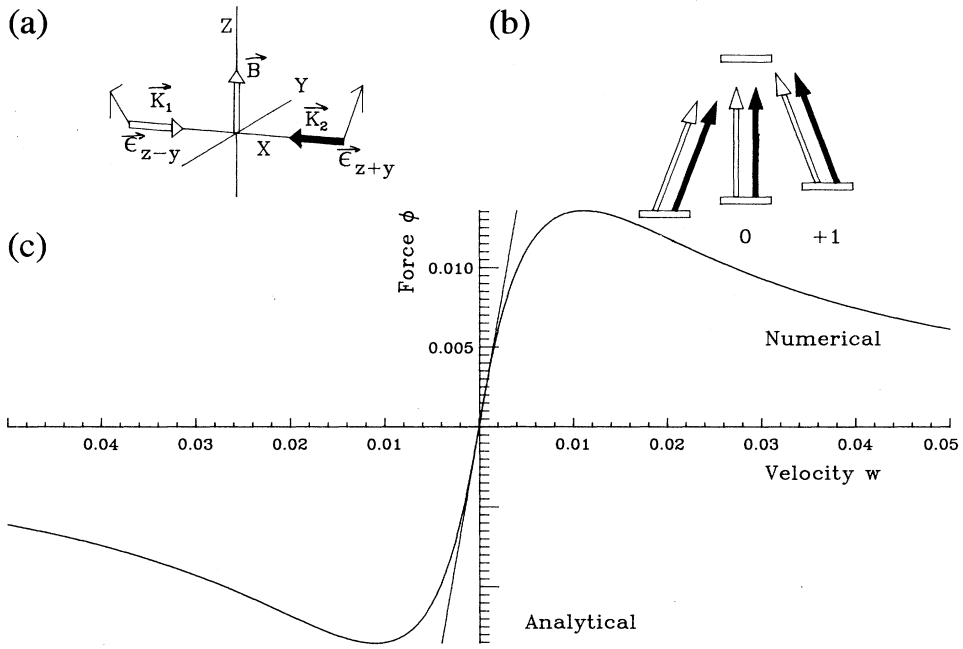

FIG. 7. The reduced force ϕ on atoms as a function of the reduced velocity w for the lin $\perp$ lin case with polarizations $\pi_{z-y} - \pi_{z+y}$ with a transverse magnetic field $\mathbf{B} = B\hat{\mathbf{z}}$ for a $J_g = 1$ to $J_e = 0$ transition. The calculation is for reduced magnetic field $b = 1$ and detuning $\Delta = -1.5\Gamma$. Since both circular polarizations have components parallel and perpendicular to $\mathbf{B}$, each light beam can induce σ_+, σ_-, and π transitions. In (b) we show the transitions that lead to the $(n = 0)$ resonances. In (c) a calculation of only the $(n = 0)$ resonance is shown and a comparison is made between the analytical result and the numerical result for this case. For the definition of b, ϕ, and w see the caption of Fig. 3.

$$\langle F_0 \rangle = -\beta v, \tag{85}$$

with the damping constant

$$\beta = \frac{9\hbar K^2 \Delta}{4\Gamma}. \tag{86}$$

Damping occurs for positive detuning in this case. In Fig. 7 we show a numerical calculation for the force in this particular case. As can be seen, damping occurs for positive detuning and the width of the resonance is again on the order of the optical pumping rate $\gamma_P \propto s_0\Gamma$. The straight line through the origin indicates the result of the analytical calculation.

The physical picture of this cooling mechanism is straightforward. The strong magnetic field averages out the optical coherences between the Zeeman sublevels. The atom is basically driven by two mutually incoherent linearly polarized standing waves with equal strengths, one polarized in the Z direction, driving the transition from the $M = 0$ sublevel, and one polarized in the Y direction, driving the transition from the sublevels $M = \pm 1$. The nodes of one of the standing waves coincide with the antinodes of the other. For positive values of the detuning, the light shifts are positive. The light shifts vary periodically over half a wavelength, and the maximal shift of the $M = 0$ state is twice the maximal shift of the $M = \pm 1$ states. The light shift of the $M = 0$

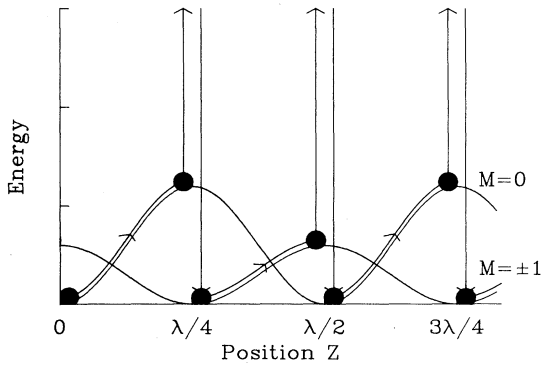

FIG. 8. The "Sisyphus" picture for the $\pi_{z-y} - \pi_{z+y}$ case with a transverse magnetic field for a $J_g = 1$ to $J_e = 0$ transition [see Fig. 7(a) for the geometry]. The standing wave of σ polarized light is out of phase with the standing wave of π polarized light and therefore the light shifts for $M = \pm 1$ are out of phase with the light shifts for $M = 0$. Since the atoms in the nodes of the π polarized light are pumped towards $M = \pm 1$ and the atoms in the nodes of the σ polarized light towards $M = 0$, atoms are preferentially pumped to states with a smaller light shift. Cooling can then only be achieved if the detuning is positive, for which this picture is drawn.

state is maximal in the nodes of the Y component of the field, where the atom tends to be pumped towards the $M = \pm 1$ states. One notices that the atom always tends to be pumped towards the state with minimal potential energy, which is the basis of the Sisyphus picture. This is illustrated in Fig. 8.

An essential ingredient of this resonance at zero velocity is the fact that the nodes of the two standing waves corresponding to the Y and the Z component of the field are displaced with respect to each other, so that the pumping scheme reverses periodically. The phase relation between the two standing waves is immaterial as a result of the rapid Larmor precession. Exactly the same result for the force arises in the case of two opposite circular polarizations of the counterpropagating waves. However, in the absence of a magnetic field, these two different configurations of orthogonal linear polarizations and opposite circular polarizations give completely different results for the forces.

III. EXPERIMENTS

A. Low-field experiments

We first review our results obtained for low magnetic fields for which the theory is described in a previous paper [11] and briefly outlined in Sec. II A. In this low-field regime we set both laser beams to have the same circular polarization and apply a magnetic field perpendicular to the direction of the laser beams [5]. As pointed out in [11], only one of the four components of the force, in this case the dipole force, can be nonzero. The force is caused by a coherent exchange of photons between the two laser beams. In the absence of a magnetic field and in the limit of low intensity, the density matrix becomes independent of the position in the standing wave and no net force on the atoms results. Thus the cooling is induced by the magnetic field and this scheme is therefore called magnetically induced laser cooling (MILC).

Since the force is purely redistributive, the scheme can be described in a "Sisyphus cooling" picture, as was done for the lin $\perp$ lin scheme [2]. The main physical idea is based on the optical pumping between differently light shifted magnetic sublevels of the atoms. Because the light is tuned below resonance, the light shifts are negative for ground-state sublevels. Thus atoms near the antinodes of the standing wave are optically pumped to the lowest sublevel (highest M_F) because of the circular polarization, and in this process, they absorb light with lower frequency than they fluoresce, thereby losing internal energy. To sustain the cooling process, atoms must be redistributed among the sublevels when the light shifts are smaller or reversed, and this is done the Larmor precession induced by the weak transverse magnetic field when an atom moves into a node where there is no optical pumping.

Moving towards the nodes increases the atomic internal energy because the negative light shift is smaller, and this increase must come at the expense of kinetic energy. Thus atoms traveling across the standing wave are optically pumped to the lowest-energy sublevel near an antinode, and redistributed among the higher sublevels near a node by Larmor precession. Of course, atoms make these transitions at a specific point in the standing wave determined by the balance between the effects of optical pumping and Larmor precession. This point is symmetric with respect to the nodes of the standing wave for atoms at rest, but moving atoms respond to the changes of the optical field amplitude in the standing wave with a certain time lag. Therefore they make transitions at a later point in their travel along the spatially dependent light shift produced by the standing wave. Thus they lose more energy than would atoms at rest on the descending part of the potential where the light shift is increasing, and gain less energy than would atoms at rest for the ascending part where the light shift is decreasing. On one cycle they lose more than they gain, and are therefore cooled. This is analogous to lin $\perp$ lin polarization gradient cooling [2], but here the Larmor precession causes the redistribution of atoms among differently light-shifted states instead of a polarization gradient.

At low fields and red detuning, the process described above cools atoms towards zero transverse velocity (see Fig. 2). If we zero the magnetic field, no cooling signal is observed as expected. If we increase the intensity of the laser, the signal increases and broadens. The measurements are in qualitative agreement with the results of numerical calculations that can be performed as described in our previous paper [11].

B. High-field experiments

At larger magnetic fields, the picture involving optical pumping and Larmor precession breaks down because these rates are no longer comparable. We arrive in a situation described in Sec. II B, where the pumping rate γ_P is small compared to the Larmor precession rate ω_Z, which in turn is small compared to the natural decay rate Γ. Sub-Doppler cooling at large fields is still observed, but it occurs around nonzero velocities $\pm v_r$ proportional to the Zeeman splitting ω_Z of the ground-state sublevels, as indicated by Eq. (25). The theory describing the results in this section is outlined in Sec. II D. We will still use a standing wave of constant circular polarization and a magnetic field transverse to the laser beams. As can be seen from one of the examples shown in Sec. II F, the theory predicts two resonances with $v_r = \pm \omega_Z / 2k$.

Our experimental results are shown in Fig. 9. The data shown in Fig. 9(a) are obtained for low magnetic field and show cooling to $v = 0$. For increasing magnetic field we observe a broadening of the peak, and eventually for high magnetic field we see two separate peaks whose splitting increases with increasing field. The transverse velocity difference between the two peaks Δv_p for several detunings and intensities for both naturally occurring isotopes of Rb fits very well to $\Delta v_p = 2v_r = \omega_Z / k$ with the appropriate g_F factor for each isotope [6]. We see excellent agreement between the predictions of the model and our measurements.

We also point out that for blue detuning (lower part of Fig. 9), slower atoms are cooled at high fields but heated at low fields. This arises because the rapid Larmor precession establishes a coherence between the ground states and is analogous to the optical coherence established be-

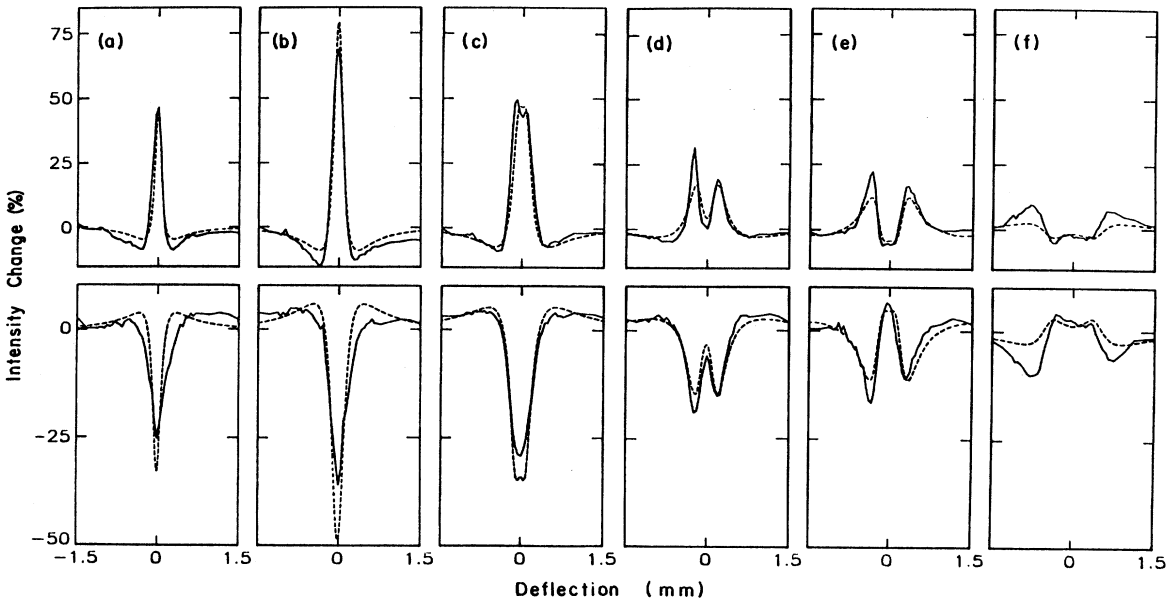

FIG. 9. A series of hot wire measurements of the atomic beam profile. The laser intensity $I = 0.25I_{\text{sat}}$ and the detuning $\Delta = -4$ MHz for the top row and $\Delta = +4$ MHz for the bottom row. The magnetic field values were (a) 57 mG, (b) 114 mG, (c) 230 mG, (d) 400 mG, (e) 570 mG, and (f) 1.14 G. The solid lines are data and the dashed lines are the numerical calculations.

tween ground and excited states by a high-intensity optical field that also produces cooling for blue detuning [16]. However, we emphasize that the present cooling is caused by ground-state coherence and is a low-intensity effect.

The dashed lines in Fig. 9 represent a theoretical calculation of the expected signal, where we averaged the intensity of the laser light over its Gaussian beam profile. In this way we can calculate both the force and the diffusion on the atoms for a fixed ratio between the Larmor precession rate and the optical pumping rate, which simplifies the calculation significantly. The velocity distribution is then calculated by numerically integrating the Fokker-Planck equation, and transforming the calculated velocity distribution to a spatial distribution for comparison with the measured signal. Despite the rather crude approximation of a constant intensity the agreement between experiment and theory is excellent.

C. Polarization gradient experiments

1. Longitudinal magnetic field

Cooling to finite velocity can also be observed if the polarization vectors of the two light beams have opposite polarization. In this section we will discuss our results when the magnetic field is in the direction of the laser beams. For an optical molasses made from opposite circular polarizations ($\sigma_+ - \sigma_-$), the theory outlined in Sec. II E applies. We expect that the atomic beam will be deflected and cooled to the transverse velocity given by $v_r' = 2v_r = \omega_Z/k$. Reversing the magnetic field deflects the atomic beam to the opposite direction. Figure 10(a)

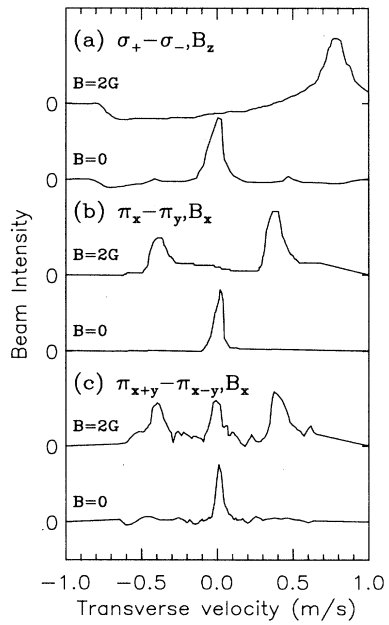

FIG. 10. Velocity distributions of ^{85}Rb atoms after passing through the optical molasses, as determined from the spatial profile measurements. The upper trace in each part is for $\mathbf{B} \neq \mathbf{0}$ and the lower one is for $\mathbf{B} = \mathbf{0}$. (a) $\sigma_+ - \sigma_-$ molasses and the magnetic field $\mathbf{B}$ along the laser axis, (b) lin $\perp$ lin and $\mathbf{B}$ along the laser polarizations, and (c) lin $\perp$ lin and $\mathbf{B}$ along the bisector of the laser polarizations. The laser parameters in all cases are $I = 3I_{\text{sat}}$ and $\Delta = -12$ MHz.

shows the velocity distribution of atoms cooled to $v = 0$ (lower trace) and to finite velocity (upper trace) determined by a $|\mathbf{B}| = 2$ G parallel to $\mathbf{k}$. Figure 2 of Ref. [7] shows a full set of such cooling and deflection peaks using the velocity-selected ^{85}Rb beam for various values of $|\mathbf{B}|$, and Fig. 3 of Ref. [7] shows the displacement Δv of those peaks vs $|\mathbf{B}|$. The data fit the straight line $\Delta v = \omega_Z/k$ to within experimental error (2%).

2. *Transverse magnetic field*

We also transversely cool the atomic motion by an optical molasses formed by two laser beams with orthogonal linear polarizations [7]. In this case we apply the magnetic field perpendicular to the laser beams and parallel to one of their polarizations. The results of Sec. II F show that atoms are cooled to $v_r = \pm\omega_Z/2k$, which is the same as in the $\sigma_+ - \sigma_+$ case, and one-half of v_r' as found in the $\sigma_+ - \sigma_-$ case. Note, however, that in this special case the force is no longer an odd function of velocity [10, 11]. The asymmetry is determined by the direction of $\mathbf{B}$; rotation of $\mathbf{B}$ by 90° about the laser axis reverses it. This is clear since reversing the atomic velocity and rotating $\mathbf{B}$ by 90° leaves the geometry unchanged.

Figure 10(b) shows the velocity distribution of atoms cooled to $v = 0$ (lower trace) and to finite velocity (upper trace) determined by a $|\mathbf{B}| = 2$ G parallel to one of the laser polarizations. Figure 4 of Ref. [7] shows a full set of measured beam profiles for various values of $\mathbf{B}$. The data show two asymmetric peaks of unequal height. Figure 5 of Ref. [7] shows the position of one of the deflected peaks vs B. Again, the data fit the VSR condition $\Delta v = \omega_Z/2k$ to within experimental error. We emphasize that the atoms are not simply deflected, but are always *cooled* to v_r with a width well below the Doppler limit.

The resonances discussed in this experimental part so far involve transitions between different Zeeman ground states [see, for instance, Fig. 3(b)]. In a polarization gradient and strong $\mathbf{B}$ field, it is also possible to have VSR that return an atom to its original Zeeman ground state, and transfer a photon from one beam to another [Fig. 7(b)]. This leads to the resonant condition $v_r = 0$, as is discussed in Sec. II C 1. We have observed this by applying $\mathbf{B}$ at 45° to both laser polarizations in the lin ⊥ lin configuration. Figure 10(c) shows the velocity distribution of atoms cooled to $v = 0$ (lower trace) and to $v = 0$ as well as $\pm v_r$ for $B = 1.93$ G (upper trace). Figure 6 of Ref. [7] shows more of these multivelocity traces with sub-Doppler spread for $B \neq 0$. The two side peaks correspond to the type of VSR shown in Fig. 3(b) and the center one, which does not shift with B, corresponds to the type shown in Fig. 7(b), and satisfies $v_r = 0$.

IV. CONCLUSIONS

We have shown that adding a magnetic field yields completely new phenomena previously unobserved in sub-Doppler laser cooling. We have provided a formal theoretical description of these phenomena that is valid for any angular-momentum scheme. Furthermore, we have observed these phenomena and compared our measurements with both the formal calculations and our simple VSR model, and have found excellent agreement. The VSR picture can be used to predict the effects for the deflection and cooling the atoms for a given direction of the magnetic field and the polarization of the light beams.

The role of the polarization gradient in previously studied cases of sub-Doppler cooling with $\mathbf{B} = \mathbf{0}$ [1,8,9,4] can now be discussed in terms of the VSR picture. With $B = 0$, the ground-state sublevels are nearly degenerate, mixed polarizations permit resonant two-photon transitions to be driven by photons from different beams, and $v_r = 0$. We point out that coherent population trapping in a three-level Λ system that cools below the recoil limit [17] is the limiting case of VSR with vanishing width. At resonance, atoms are in a coherent superposition of atomic ground states that cannot absorb light.

Finally we propose some applications of cooling to nonzero velocity. If the deflection is applied to a decelerated beam, it is a superb method for extracting or steering a well-defined cold beam. Also, one could imagine building an atomic storage ring based on this deflecting and cooling technique that could provide a beam that is ideal for precision spectroscopy, the study of cold collisions, and collective effects of cold atoms.

ACKNOWLEDGMENTS

This work supported by the NSF and the ONR. P.V.D.S. was supported by K.N.A.W., the Netherlands.

* Present address: Room 204, Bldg. 88, Lawrence Berkeley Laboratory, Berkeley, CA 94720.

† Present address: Fakultat für Physik, Universitat Bielefeld, Bielefeld, Germany.

[1] P. Lett *et al.*, Phys. Rev. Lett. **61**, 169 (1988).
[2] J. Dalibard and C. Cohen-Tannoudji, J. Opt. Soc. Am. B **6**, 2023 (1989).
[3] P. Ungar *et al.*, J. Opt. Soc. Am. B **6**, 2058 (1989).
[4] C. Salomon *et al.*, Europhys. Lett. **12**, 683 (1990).
[5] B. Sheehy *et al.*, Phys. Rev. Lett. **64**, 858 (1990).
[6] S-Q. Shang *et al.*, Phys. Rev. Lett. **65**, 317 (1990).
[7] S-Q. Shang *et al.*, Phys. Rev. Lett. **67**, 1094 (1991).
[8] D. Weiss *et al.*, J. Opt. Soc. Am. B **6**, 2072 (1989).
[9] P. Lett *et al.*, J. Opt. Soc. Am. B **6**, 2084 (1989).
[10] G. Nienhuis, in *Proceedings of the Conference on Light Induced Kinetic Effects*, edited by L. Moi and E. Arimondo (ETS Editrice, Pisa, 1991), p. 139.
[11] G. Nienhuis, P. van der Straten, and S.-Q. Shang, Phys. Rev. A **44**, 462 (1991).
[12] P. Berman, in *Proceedings of the Conference on Light Induced Kinetic Effects* (Ref. [10]), p. 149.
[13] G. Nienhuis, Phys. Rep. **138**, 151 (1986).
[14] M. Walhout, J. Dalibard, S. L. Rolston, and W. D. Phillips, J. Opt. Soc. Am. **9**, 1997 (1992).
[15] A. Kastler, C. R. Acad. Sci. Paris **271**, 999 (1970).
[16] A. Aspect *et al.*, Phys. Rev. Lett. **57**, 1688 (1986).
[17] A. Aspect *et al.*, Phys. Rev. Lett. **61**, 826 (1988).